Obtaining Frequency Responses of User-Defined Models in the ATP

Sergio L. Varricchio, *Senior, IEEE*, and Thomas M. Campello, *Member, IEEE*

***Abstract*—User-Defined Models (UDMs) in the Alternative Transients Program (ATP) are valuable tools. However, its creation using the ATP MODELS language is not simple. One type of UDM of particular importance is the high-fidelity Frequency-Dependent Network Equivalent (FDNE), assembled, in general, by fitting the Frequency Responses (FRs) of the self-and transfer admittances seen from the boundary buses of the external area (part of the system to be substituted by the FDNE). The correctness of the FDNE implementation can be verified by comparing its FRs with those of the external area. Unfortunately, obtaining the FRs of a UDM is not a simple task as in the case of the ATP built-in components. Thus, this work proposes a method for calculating the FRs of the UDMs implemented with the MODELS in the ATP. The proposal is based on the UDM time responses to the unit impulse in symmetric components and the Fourier transform.**

Link to graphical and video abstracts, and to code: https://latamt.ieeer9.org/index.php/transactions/article/view/9654

***Index Terms*—ATP Models; Frequency-Dependent Network Equivalent (FDNE); Frequency response; Numerical Fourier transform; Symmetrical components of non-sinusoidal inputs.**

I. Introduction

THE models language [1] available in the Alternative Transients Program (ATP) [2] is a valuable tool used for the implementation of User-Defined Models (UDMs) in several different applications, such as environment simulation for distance protection [3], power transformer modeling [4], differentiator-smoother filter implementation [5], and grid-following and grid-forming power converter modeling [6]. Finally, an important MODELS utilization is to build Frequency-Dependent Network Equivalents (FDNEs) [7, 8, 9].

Electromagnetic Transient (EMT) studies usually concentrate on some specific part of the power system in which an electrical phenomenon is of concern. Hence, it is possible to divide the network into two areas. One is the study area (area under investigation that must be modeled in detail); and the other is the remaining system (or external area) that can be represented by a suitable equivalent for observing transients' phenomena [9].

The most used equivalent is the short-circuit equivalent. There are many commercial tools available that aid to build these equivalents, but they are not very accurate for frequencies other than the network's nominal frequency [9]. Other kind of equivalent is the FDNEs, that retains the external area characteristics for a wide band of frequencies, ensuring higher fidelity (accuracy) than the short-circuit equivalent.

The Vector Fitting (VF) algorithm [10] is an effective method for obtaining FDNEs in the format of Rational Models (RMs) [7, 9, 11, 12] by fitting the Frequency Responses (FRs) of the Transfer Functions (TFs) of the external area boundary buses, computing their approximate dominant poles and associated residues. With the set of poles and residues, a Rational Model (RM) is assembled to represent the external area.

To initiate the creation of an FDNE, the first step is to split the system into two parts: the study area and the external area. Subsequently, the external area is modeled, and the FRs of the self and transfer admittances seen from the boundary buses are computed, considering both the positive and zero sequences. The VF is then employed to obtain the RM. Once this is accomplished, the RMs passivity is verified (and enforced if necessary). The last step is the FDNE implementation in a EMT simulation software, like the ATP using the MODELS.

As in every computational implementation, validating the MODELS code holds significant importance. The main method for validating FDNEs involves comparing the calculated FRs of each sequence component of the external area with those fitted by VF. While ATP easily allows users to conduct simulations in either time or frequency domains for networks represented by the interconnection of built-in elements, the MODELS component inadequately works during frequency domain simulations. Consequently, employing this standard tool for such validations becomes unfeasible.

One option is to validate the MODELS in the time domain by comparing the responses of the FDNE and the external area. This approach can be unworkable when it is necessary to model a large external area in EMT simulation software. Alternatively, FRs can be indirectly obtained by applying time-domain inputs to the FDNE and, in a second stage, a Fourier Transform Algorithm (FTA) to its outputs. In the time-domain input stage, the more common method to obtain these FRs is the application of sinusoidal inputs with different frequencies [13]. However, this method is computationally inefficient, given that the FDNE typically represents a wide range of frequencies (ranging from a few tens of Hz up to the order of MHz), implying a

The associate editor coordinating the review of this manuscript and approving it for publication was Mario R. Arrieta Paternina (*Corresponding author: Thomas Campello*).

S. L. Varricchio, Independent Consultant, Rio de Janeiro, RJ, Brasil (e-mail: slvarricchio@gmail.com).

Thomas M. Campello, Centro Federal de Educação Tecnológica Celso Suckow da Fonseca, Rio de Janeiro, Brasil (e-mail: thomas.campello@cefet-rj.br).

considerable number of sinusoidal sources and, consequently, a high CPU time.

The FTA applied in the time domain responses of the UDM is a crucial stage in obtaining the FRs. The FFTW is one the most used FTA algorithms, proposed in 1998 [14] and continually maintained. Its latest publication in the literature was in 2007 [15]. This algorithm is available in the more significant scientific prototyping computational tools like Matlab software [16]. While it offers computational efficiency across a wide range of applications, it demands prior problem parameterization from the user. A lack of user proficiency in this task can lead to inaccurate results. Although the theory of the Fourier transform is widely known, its computational implementation remains a highly discussed topic, with several recent important publications, each one addressing specific implementations for particular problems, such as broadband signal modulation and signal processing for advanced wireless communications systems [17, 18], or novel numerical methods for calculating this transform, such as through hyperfunctions theory [19].

This work proposes a methodology for calculating the FRs of the FDNE, or any other UDM, implemented with the MODELS in the ATP. To achieve this contribution, firstly the paper extends the concept of symmetrical components to non-sinusoidal inputs, allowing obtaining the positive and zero sequence FRs by applying an approximate unit impulse in UDM and the Fourier transform in its output. Thus, instead of multiple sinusoidal inputs, a balanced three-phase impulse is used, followed by a Fourier Transform to obtain accurate positive and zero sequence frequency responses, which is more efficient and highly accurate. Secondly, the paper also proposes a Numerical Fourier Transform Algorithm (NFTA) based on balanced three-phase impulse response characteristics, which is computationally efficient and eliminates the need for pre-parameterization time domain data to work correctly, making it more user-friendly and accurate.

II. METHODOLOGY

In the following subsections, some concepts and definitions that underpin the proposed methodology are established in detail. For space-saving, the emphasis here is on the positive sequence, but the extension to the zero sequence is straightforward.

A. Representation of Non-Sinusoidal Inputs in Symmetrical Components

A generic real function f can be represented by:

$$f(t) = \Re\{F(t)\} = \Re\{\tilde{F}(t)\, e^{j\omega t}\} = \Re\{F_A(t)\, e^{j\theta} e^{j\omega t}\} \quad (1)$$

where $F_A(t)$ is a real or complex amplitude function. This representation allows the definition of a generic balanced three-phase voltage (positive sequence) input [20] with waveforms not restricted to cosine forms, given by:

$$\begin{bmatrix} v_a(t) \\ v_b(t) \\ v_c(t) \end{bmatrix} = \Re\left\{\begin{bmatrix} V_a(t) \\ V_b(t) \\ V_c(t) \end{bmatrix}\right\} = \Re\left\{\begin{bmatrix} 1 \\ a^2 \\ a \end{bmatrix} \tilde{V}(t)\, e^{j\omega t}\right\} \quad (2)$$

where $a = e^{j120^\circ}$ and

$$\tilde{V}(t) = V_A(t)\, e^{j\theta} \quad (3)$$

Like $F_A(t)$, $V_A(t)$ can be a real or a complex function.

Substituting $V_A(t) = \delta(t)$ and $\theta = 0$ into (3), one obtains:

$$\tilde{V}(t) = \delta(t) \quad (4)$$

where $\delta(t)$ is the unit impulse function. Substituting (4) and $\omega = 0$ into (2), the balanced three-phase unit impulse voltage input is obtained:

$$\begin{bmatrix} v_a(t) \\ v_b(t) \\ v_c(t) \end{bmatrix} = \Re\left\{\begin{bmatrix} V_a(t) \\ V_b(t) \\ V_c(t) \end{bmatrix}\right\} = \Re\left\{\begin{bmatrix} 1 \\ a^2 \\ a \end{bmatrix} \delta(t)\right\} = \begin{bmatrix} 1 \\ -0.5 \\ -0.5 \end{bmatrix} \delta(t) \quad (5)$$

Considering an integration step Δt, the unit impulse in the time domain can be approximated by the triangular function shown in Fig. 1.

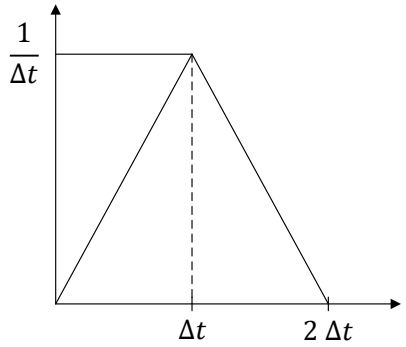

Fig. 1. Approximation of the unit impulse by a triangular function.

The application of a balanced three-phase unit impulse voltage input in a UDM, implemented using the type-94 component of the ATP MODELS language, is shown in Fig. 2.

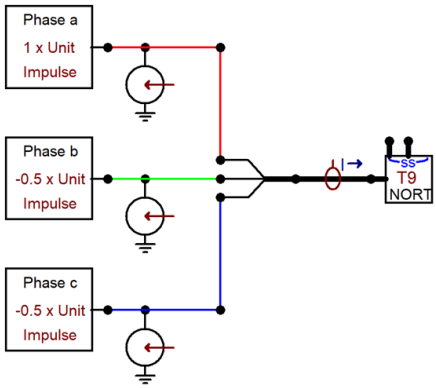

Fig. 2. Application of a balanced three-phase unit impulse voltage input in an ATP UDM.

B. The Unit Impulse Response

The Fourier transform of (5) is given by:

$$\begin{bmatrix} v_a(j\omega) \\ v_b(j\omega) \\ v_c(j\omega) \end{bmatrix} = \Re\left\{\begin{bmatrix} V_a(j\omega) \\ V_b(j\omega) \\ V_c(j\omega) \end{bmatrix}\right\} = \Re\left\{\begin{bmatrix} 1 \\ a^2 \\ a \end{bmatrix}\right\} = \begin{bmatrix} 1 \\ -0.5 \\ -0.5 \end{bmatrix} \quad (6)$$

The relationship between the voltage input given in (6) and the UDM current response is defined by the nodal admittance matrix seen from the interested three-phase bus. For a balanced system, one has:

$$\begin{bmatrix} i_a(j\omega) \\ i_b(j\omega) \\ i_c(j\omega) \end{bmatrix} = \begin{bmatrix} y_s(j\omega) & y_m(j\omega) & y_m(j\omega) \\ y_m(j\omega) & y_s(j\omega) & y_m(j\omega) \\ y_m(j\omega) & y_m(j\omega) & y_s(j\omega) \end{bmatrix} \begin{bmatrix} 1 \\ -0.5 \\ -0.5 \end{bmatrix} \quad (7)$$

where y_s and y_m denote the self- and transfer impedance of the three-phase bus. After some simple algebraic manipulations, one obtains:

$$\begin{bmatrix} i_a(j\omega) \\ i_b(j\omega) \\ i_c(j\omega) \end{bmatrix} = \begin{bmatrix} 1 \\ -0.5 \\ -0.5 \end{bmatrix} y_+(j\omega) \quad (8)$$

where $y_+(j\omega)$ is the positive sequence admittance seen from the currents, given by:

$$y_+(j\omega) = y_s(j\omega) - y_m(j\omega) \quad (9)$$

Taking the inverse Fourier transform of (8), yields:

$$\begin{bmatrix} i_a(t) \\ i_b(t) \\ i_c(t) \end{bmatrix} = \begin{bmatrix} 1 \\ -0.5 \\ -0.5 \end{bmatrix} \mathcal{F}^{-1}\{y_+(j\omega)\} \quad (10)$$

Comparing (10) with (5), it can be seen that the output keeps the same phase magnitude proportionality as the input. This fact can be verified in Fig. 3, which represents the current response due to the application of a balanced three-phase unit impulse voltage input in the FDNE described in Section III, valid in the frequency range from 0 to 1.2 kHz.

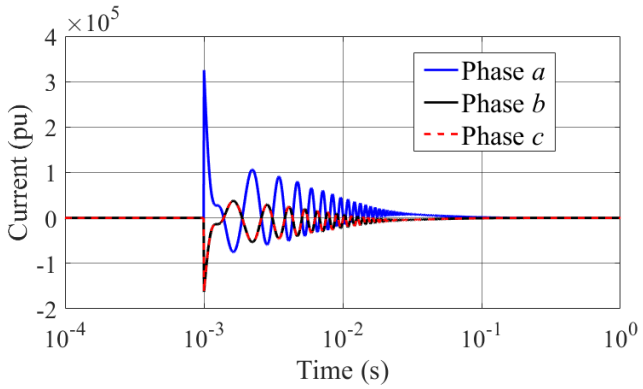

Fig. 3. Current responses due to the application of a balanced three-phase unit impulse voltage input at 10^{-3} s in the 0 to 1.2 kHz FDNE.

From (10), the positive sequence admittance FR can be computed by:

$$y_+(j\omega) = \mathcal{F}\{i_a(t)\} \quad (11)$$

Thus, after applying the three-phase positive sequence unit impulse voltage input $[1 \quad -0.5 \quad -0.5]^T\,\delta(t)$ (the superscript ^{T} denotes matrix or vector transpose) at the interface node of the MODELS, the current vector $[i_a(t) \quad i_b(t) \quad i_c(t)]^T$ is obtained. Next, the positive sequence admittance FR $y_+(j\omega)$ is computed by the Fourier transform of the current in phase a, as indicated in (11).

Analogously to (5) and (10) the zero sequence unit impulse voltage input and its corresponding current output is given, respectively, by:

$$\begin{bmatrix} v_{a0}(t) \\ v_{b0}(t) \\ v_{c0}(t) \end{bmatrix} = \begin{bmatrix} 1 \\ 1 \\ 1 \end{bmatrix} \delta(t) \quad (12)$$

$$\begin{bmatrix} i_{a0}(t) \\ i_{b0}(t) \\ i_{c0}(t) \end{bmatrix} = \begin{bmatrix} 1 \\ 1 \\ 1 \end{bmatrix} \mathcal{F}^{-1}\{y_0(j\omega)\} \quad (13)$$

where $y_0(j\omega)$ is the zero sequence admittance seen from the currents, given by:

$$y_0(j\omega) = y_s(j\omega) + 2y_m(j\omega) \quad (14)$$

From (13), the zero sequence admittance FR can be computed by:

$$y_0(j\omega) = \mathcal{F}\{i_{a0}(t)\} = \mathcal{F}\{i_{b0}(t)\} = \mathcal{F}\{i_{c0}(t)\} \quad (15)$$

C. Numerical Fourier Transform

Fig. 4 shows the linear approximation of a time function $f(t)$ in the interval $[t_i,\ t_{i+1}]$.

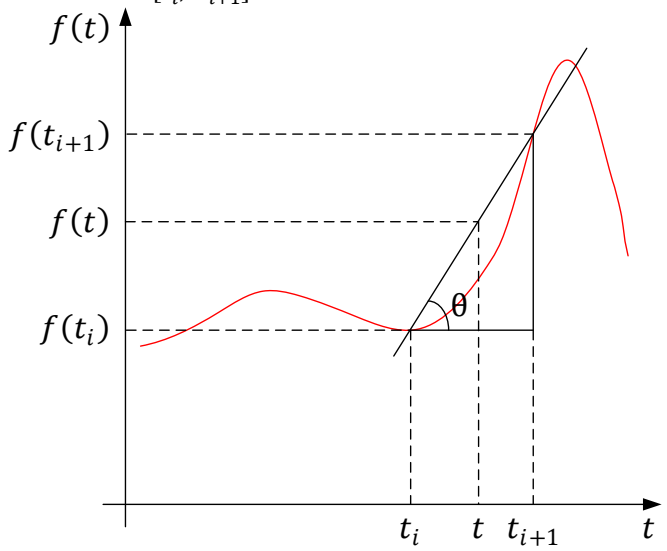

Fig. 4. Linear approximation of $f(t)$ in the interval $[t_i,\ t_{i+1}]$.

According to this figure, one has:

$$\frac{f(t) - f(t_i)}{t - t_i} = \frac{f(t_{i+1}) - f(t_i)}{t_{i+1} - t_i} = \tan\theta \quad (16)$$

where $(t, f(t))$ represents a generic point on the linear approximation of the function, which can be written as:

$$f(t) = \tan\theta\,(t - t_i) + f(t_i) \quad (17)$$

The Fourier transform $F(j\omega)$ of $f(t)$ is given by [21]:

$$F(j\omega) = \int_{-\infty}^{\infty} f(t)\, e^{-j\omega t} dt \quad (18)$$

According to (18), the contribution of the interval $[t_i,\ t_{i+1}]$ to $F(j\omega)$, considering the linear approximation (17), is given by:

$$\Delta F_i(j\omega) = \tan\theta \int_{t_i}^{t_{i+1}} t\, e^{-j\omega t} dt + [f(t_i) - \tan\theta\, t_i] \int_{t_i}^{t_{i+1}} e^{-j\omega t} dt \quad (19)$$

To perform the integration, (19) can be rewritten as:

$$\Delta F_i(j\omega) = -\frac{\tan\theta}{\omega^2}\int_{t_i}^{t_{i+1}} (-j\omega t)\, e^{-j\omega t} d(-j\omega t) + j\left(\frac{f(t_i) - \tan\theta\, t_i}{\omega}\right)\int_{t_i}^{t_{i+1}} e^{-j\omega t} d(-j\omega t) \quad (20)$$

From [22], one has:

$$\int_{t_i}^{t_{i+1}} e^{-j\omega t} d(-j\omega t) = e^{-j\omega\, t_{i+1}} - e^{-j\omega\, t_i} \quad (21)$$

$$\int_{t_i}^{t_{i+1}} (-j\omega t)\, e^{-j\omega t} d(-j\omega t) = e^{-j\omega\, t_{i+1}}(-j\omega\, t_{i+1} - 1) - e^{-j\omega\, t_i}(-j\omega\, t_i - 1) \quad (22)$$

Substituting (21) and (22) into (20), yields:

$$\Delta F_i(j\omega) = \frac{\tan\theta}{\omega^2}[e^{-j\omega\, t_{i+1}}(j\omega\, t_{i+1} + 1) - e^{-j\omega\, t_i}(j\omega\, t_i + 1)] + j\left(\frac{f(t_i) - \tan\theta\, t_i}{\omega}\right)(e^{-j\omega\, t_{i+1}} - e^{-j\omega\, t_i}) \quad (23)$$

Finally, $F(j\omega)$ can be approximated by:

$$F(j\omega) \cong \sum_{i=1}^{n_{\Delta t}} \Delta F_i(j\omega) \quad (24)$$

with:

$$n_{\Delta t} = n_t - 1 \quad (25)$$

where $n_{\Delta t}$ and n_t denote, respectively, the numbers of subintervals and time instants considered.

Equation (23) can be simplified with consequent and significant improvement in its computational performance, using the following relationships:

$$e^{-j\omega\, t_{i+1}} = e^{-j\omega t_i}\, e^{-j\omega\Delta t} \quad (26)$$

$$j\omega\, t_{i+1} = j\omega\,(t_i + \Delta t) = j\omega t_i + j\omega\Delta t \quad (27)$$

$$j\frac{\tan\theta\, t_i}{\omega} = \frac{\tan\theta}{\omega^2} j\omega t_i \quad (28)$$

Substituting (26), (27) and (28) into (23) and after some algebraic manipulations, one has:

$$\Delta F_i(j\omega) = e^{-j\omega t_i}\left\{\frac{\tan\theta}{\omega^2}[(e^{-j\omega\Delta t} - 1) + e^{-j\omega\Delta t} j\omega\Delta t] + j\frac{f(t_i)}{\omega}(e^{-j\omega\Delta t} - 1)\right\} \quad (29)$$

The computational performance of the Fourier transform can be further improved considering that, in general, the response $f(t)$ to the unit impulse presents a fast initial oscillation of large amplitude, quickly falling to values close to zero (see Fig. 3). Thus, from a specific time point t_{cut} onwards, the contributions $\Delta F_i(j\omega)$ to $F(j\omega)$ can be neglected. The determination of t_{cut} can be carried out, for example, by taking five points $\omega_k, (k = 1, \cdots, 5)$ on the $j\omega$ axis (including the initial and final frequency values) logarithmically spaced. At these five points, the calculation of $F(j\omega)$ is, firstly, made considering the entire time interval provided, from the instant of the impulse application until t_{max}. Next, the calculation is carried out again until the time instant (t_{cut}), in which the maximum relative percentage error (ε) among these five points satisfies a selected tolerance (tol). Mathematically, one has:

$$\varepsilon = \max\left(\left|\frac{F_{t_{max}}(j\omega_k) - F_{t_{cut}}(j\omega_k)}{F_{t_{max}}(j\omega_k)}\right|\right) \times 100\% \leq tol \quad (30)$$

where $F_{t_{max}}(j\omega_k)$ and $F_{t_{cut}}(j\omega_k)$ denote, respectively, the values of $F(j\omega)$ calculated at points $\omega_k, (k = 1, \cdots, 5)$, considering all time instants up to t_{max} and only up to t_{cut}.

After the t_{cut} value determination, $F(j\omega)$ is efficiently calculated for all desired frequency points using t_{cut}. The pseudocode for the proposed Fourier transform is presented in Algorithm 1.

Algorithm 1: Fourier Transform.

Input for the first call: Δt, $n_{\Delta t}$, t, $f(t)$, ω_k (number of input arguments: $nargin = 5$).
Output of the first call: $F = F_{t_{max}}$.
Input for the second call: Δt, $n_{\Delta t}$, t, $f(t)$, ω, $F_{t_{max}}$, tol (number of input arguments: $nargin = 7$).
Output of the second call: $F = F_{t_{cut}}$.

```
Set F = 0
for i = 1 to n_Δt do
  Compute tan θ using (16)
  Compute ΔF_i using (29) and considering ω as a vector
  Compute e^{-jωt_{i+1}} = e^{-jωt_i} e^{-jωΔt}
  Set F = F + ΔF_i
  if (nargin > 5) then
    Compute the relative percentage error ε using (30)
    if (ε ≤ tol) then
      skip the for loop
    end if
  end if
end for
return F
```

III. On using the Triangular Function

From Fig. 1, it is easy to see that the smaller the value of Δt, the better $f_\Delta(t)$ approximates $\delta(t)$. Therefore, the value of Δt should be determined so that $f_\Delta(t)$ is a good approximation to $\delta(t)$ but is not unnecessarily too small to compromise CPU time. Suitable determination of Δt can be accomplished using the Laplace transformation of $f_\Delta(t)$, given by:

$$\mathcal{L}\{f_\Delta(t)\} = f_\Delta(s, \Delta t) = \frac{1}{\Delta t^2\, s^2}[1 - 2e^{-\Delta t\, s} + e^{-2\Delta t\, s}] \quad (31)$$

The modulus FR of the triangular function $f_\Delta(j\omega, \Delta t)$ is shown in Fig. 5 for two Δt values: 100 μs and 1 μs. As one can see, for $\Delta t = 1$ μs, the function $f_\Delta(j\omega, 1\mu s)$ has the same modulus FR as the unit impulse $\delta(j\omega)$, meaning that $f_\Delta(j\omega, 1\mu s)$ can excite all UDM frequencies with the same strength.

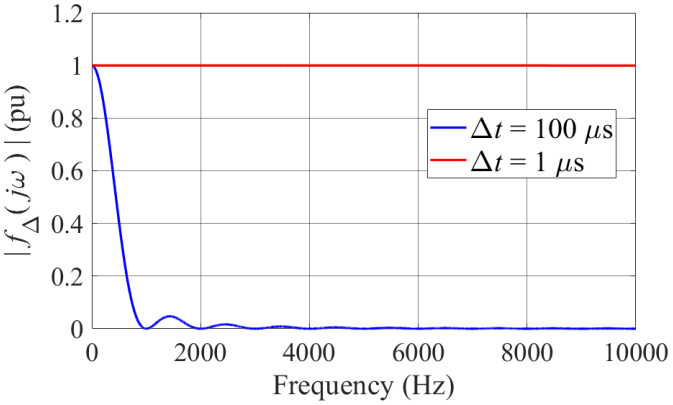

Fig. 5. Modulus FRs of the triangular function $f_\Delta(j\omega, \Delta t)$.

Unlike $\delta(j\omega)$, the angle of $f_\Delta(j\omega, 1\mu s)$ is not null for all frequencies, as pictured in Fig. 6.

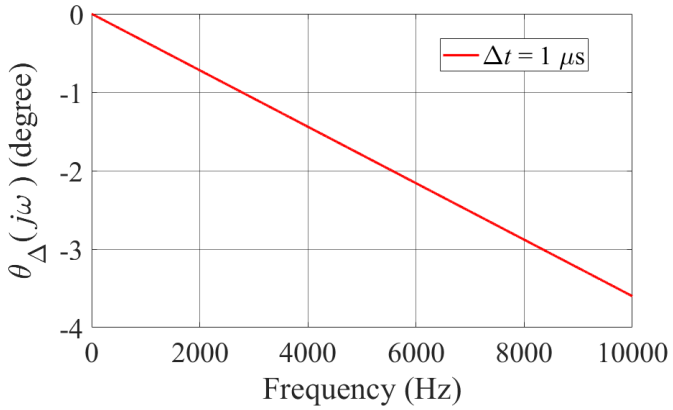

Fig. 6. Angle FR of the triangular function $f_\Delta(j\omega, 1\mu s)$.

Note that to validate the UDM MODELS code, the UDM and the external area FRs, G and H, respectively, must be compared. The FR H is obtained, in general, by a harmonic frequency scan program. On the other hand, G can be obtained from G_Δ, which denotes the UDM FR to $f_\Delta(j\omega, 1\mu s)$. In other words, G denotes y_+ or y_0, given by (11) and (15), respectively. However, in practice, the input provided is a triangular waveform that approximates an impulse, thus what is obtained after the Fourier transform is G_Δ that must be corrected to get G.

The UDM response to $f_\Delta(j\omega, 1\mu s)$ is given by $G_\Delta = G\, f_\Delta(j\omega, 1\mu s)$, thus:

$$G = \frac{G_\Delta}{f_\Delta(j\omega, 1\mu s)} \tag{32}$$

Considering that $|f_\Delta(j\omega, 1\mu s)| = 1$, in the polar form $f_\Delta(j\omega, 1\mu s)$ can be written as:

$$f_\Delta(j\omega, 1\mu s) = e^{j\theta_\Delta} \tag{33}$$

where θ_Δ is depicted in Fig. 6. Substituting (33) into (32), one has:

$$G = \frac{G_\Delta}{e^{j\theta_\Delta}} \tag{34}$$

Equation (34) shows that the UDM FR, i.e. the UDM impulse response, can be easily obtained from the UDM response to $f_\Delta(j\omega, 1\mu s)$. If the triangular function is applied at a non-zero instant t_a, by the time shifting property, (9) should be replaced by:

$$G = \frac{G_\Delta}{e^{j(\theta_\Delta - \omega t_a)}} \tag{35}$$

A block diagram illustrating the proposed methodology to validate UDM model codes in the ATP is presented in Fig. 7.

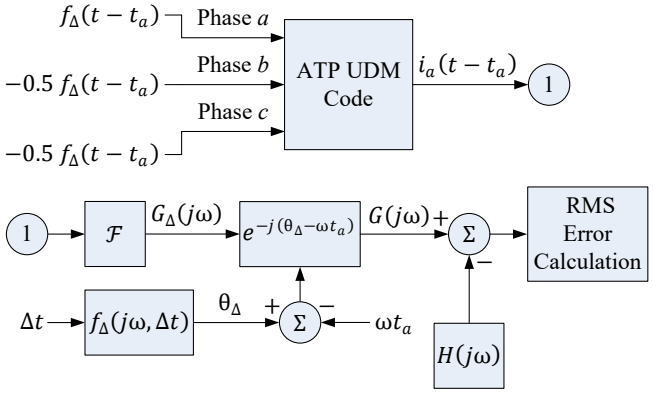

Fig. 7. Block diagram illustrating the proposed methodology.

IV. Tests and Results

A. One-port FDNE Results

A one-port FDNE of the Brazilian Interconnected Power System (BIPS), implemented in the ATP MODELS, was used to validate the proposed methodology.

The bus 431, representing a 230 kV substation, was selected as the boundary bus. The external area comprises the entire BIPS transmission system, consisting of 9497 buses, 7809 transmission lines, 2229 generators, and 3694 transformers. Due to its size, it becomes impractical to fully represent it in ATP. The study area is a distribution network, whose detailed representation is beyond the scope of this work.

The FDNE was built using the positive sequence FR of the self-admittance seen from the boundary bus, calculated using a harmonic frequency scan program fed by the network database (complete model), freely available on the Brazilian Power System Operator's website [23]. Subsequently, the RM (FDNE) is obtained using the VF to fit the FR. Finally, the FDNE is implemented in the ATP MODELS following the methodology described in [7] and [8]. Since only one boundary bus (Single-Input Single-Output - SISO TF) was considered, the RM is naturally passive, not requiring passivity verification and enforcement.

VF requires that the user provide some input parameters: the calculated values of the TFs to be fitted, frequency range of interest, weight for each sampled point, number of iterations to be performed, and a set of initial poles. Therefore, in these tests, all weights were considered unitary, the initial poles were defined as guided in [10], the TF was calculated as previously mentioned, and two frequency ranges of interest were considered: the first one from 0 to 1.2 kHz and the second from 0 to 10 kHz, thus generating two MRs and two MODELS implementations.

The proposed methodology was implemented in three MODELS, one for each phase, and connected at the FDNE MODELS terminals, as shown in Fig. 2. Fig. 3 and Fig. 8 show the current responses of the FDNE MODELS considering the frequency ranges from 0 to 1.2 kHz and from 0 to 10 kHz, respectively. Fig. 9 shows the zoom of the Fig. 8 curves.

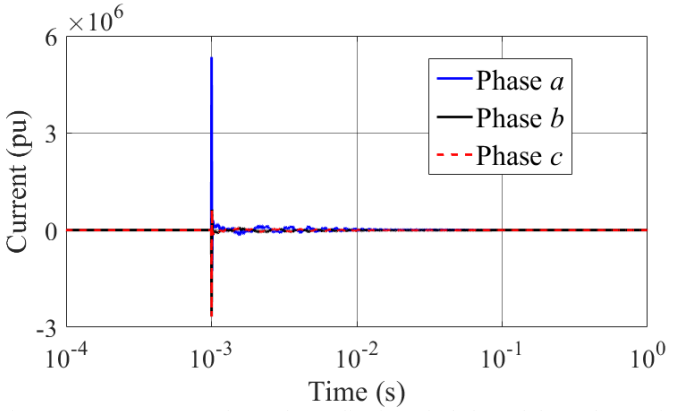

Fig. 8. Current responses due to the application of a balanced three-phase unit impulse voltage input at 10^{-3} s in the 0 to 10 kHz FDNE.

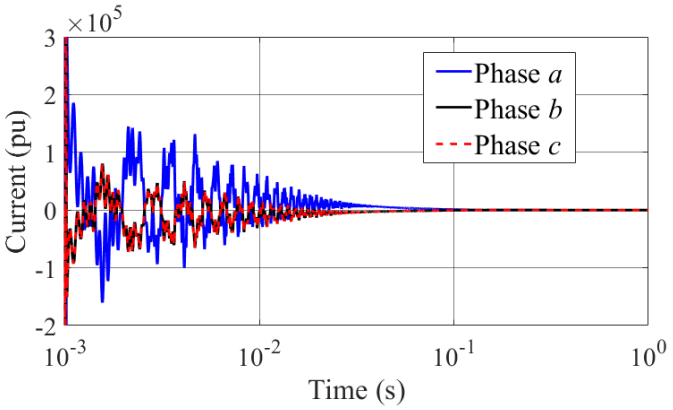

Fig. 9. Zoom of the Fig. 8 curves.

Next, the NFTA was applied to the phase *a* of these current response curves, considering an error tolerance of 0.1% (see (30)). Fig. 10 and Fig. 11 show, respectively, the modulus and angle FRs from 0 to 10 kHz of the complete model, in black, and of the 0 to 1.2 kHz and 0 to 10 kHz FDNEs in blue and dashed red, respectively. Note that the FR of the 0 to 1.2 kHz FDNE deviates considerably from the complete model FR at frequencies beyond this range. This is an expected behavior since the VF only ensures a good FR fitting in the frequency range considered in the construction of the FDNE.

The most common method in the literature to test this kind of UDM is injecting sinusoidal voltage or current sources at the exact frequency of interest. In this case, to validate the FDNE MODEL considering a range from 0 to 10 kHz, using a step of 1 Hz, it should be necessary to include 10.000 sources, one at each interest frequency and each phase. This methodology was implemented using MODELS to compare its computational performance with the proposed method. It should be noted that the sinusoidal source method required a simulation time of 2 seconds to achieve a similar level of accuracy (in terms of RMS error) as the proposed method, whereas only 1 second was sufficient for the unit impulse application.

Considering the computational performance,

TABLE shows the CPU time consumed by the ATP using the sinusoidal source method with their frequencies varying in steps of 1 Hz, 10 Hz, and 100 Hz, and using the unit impulse method. This time consumption was observed using a PC running a Windows 10 64-bit system equipped with an Intel Core i5 3.2 GHz and 8 GB of RAM. Observe that in the proposed method it is not needed to specify any frequency step.

TABLE also shows the RMS error (%) obtained by:

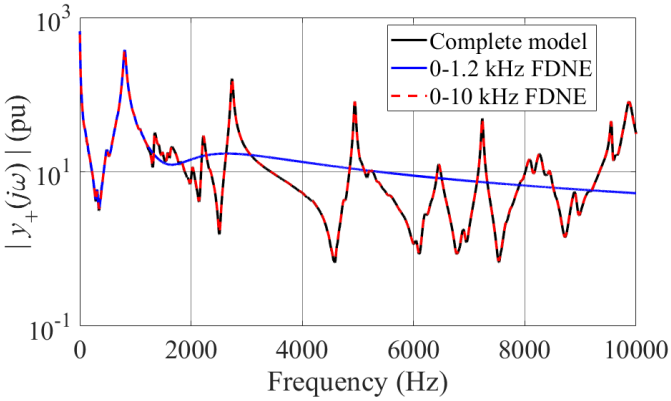

Fig. 10. Positive sequence modulus FRs of the complete model and of the FDNEs.

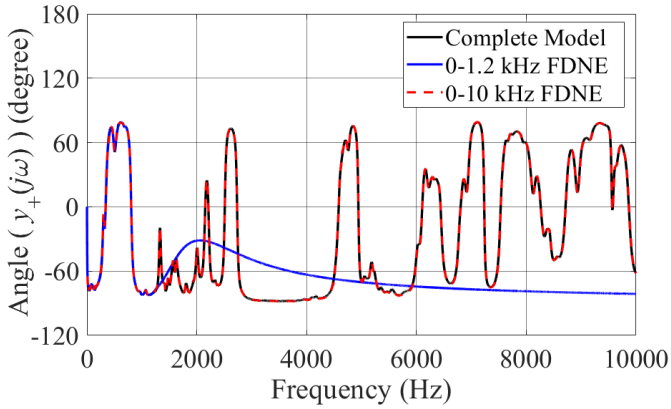

Fig. 11. Positive sequence angle FRs of the complete model and of the FDNEs.

$$\varepsilon_{RMS} = \sqrt{\frac{\sum_{m=1}^{N_s} |\varepsilon(s_m)|^2}{\sum_{m=1}^{N_s} |h(s_m)|^2}} \tag{36}$$

with

$$\varepsilon(s_m) = \tilde{h}(s_m) - h(s_m) \tag{37}$$

where $\tilde{h}$ is the FR obtained after applying the FTA, h is the reference FR, and s_m is one of the N_s frequency samples.

TABLE I
ATP TIME CONSUMPTION USING THE SINUSOIDAL SOURCE AND THE PROPOSED METHODS

	Sinusoidal Sources Method			Unit. Impulse
	Step			
	1 Hz	10 Hz	100 Hz	-
ATP CPU time consumed (hours)	16:05	03:38	01:45	00:31
RMS Erros (%)	1.75	7.27	67.92	1.62

TABLE I shows that the accuracy of the traditional method using a source frequency step of 1 Hz is similar to that of the proposed method. However, the required CPU time is 31 times higher. Increasing the frequency step size reduces the overall simulation time. Nevertheless, it also leads to a higher RMS error, as the larger spacing between frequency points may cause sharp peaks in the response to be missed. Considering the proposed NFTA, implemented in C language, consumed approximately 5 seconds of CPU time to obtain each one of these FRs, against 2 seconds, approximately, of the Matlab built-in FFTW algorithm. Although the built-in MATLAB function executes faster, it is essential to consider the time required to prepare the input data for its use, which is not accounted for in this time analysis. The decision was made to implement NFTA in C due to the high computational performance that this language offers. In the future, it is intended to analyze, in terms of language resources and computational performance, the feasibility of this implementation directly in the Models.

Returning to the proposed method, the NFTA was applied in current responses with 1 s duration and 1 μs integration step, totaling 1 000 001 points, demonstrating its high efficiency. Note that the integrations were performed for 10 000 frequency points for each FR.

B. Two-port FDNE Results

To exemplify the methodology applied to a two-port FDNE, the 77-bus electrical network, shown in Fig. 12, was used. The study area is shown in blue, the external area in black, and the boundary buses in red. This system consists of 10 three-winding transformers, 22 two-winding transformers, 29 generators, 34 loads, 35 short TLs (modeled with one RLC-pi circuit), and 30 long TLs (represented by Bergeron's model).

Considering the selected set of boundary buses, the two areas (study and external areas) are split, and the admittance MIMO TF matrix of the positive sequence is calculated for the external area with all voltage and current sources deactivated. The FDNE of the external area was built considering the frequency range of interest from 10 to 10 kHz [9].The implemented UDM can be tested as illustrated in Fig. 13. In this case, to compute the admittance FRs, a balanced three-phase unit impulse voltage input is applied to one port while the other is short-circuited.

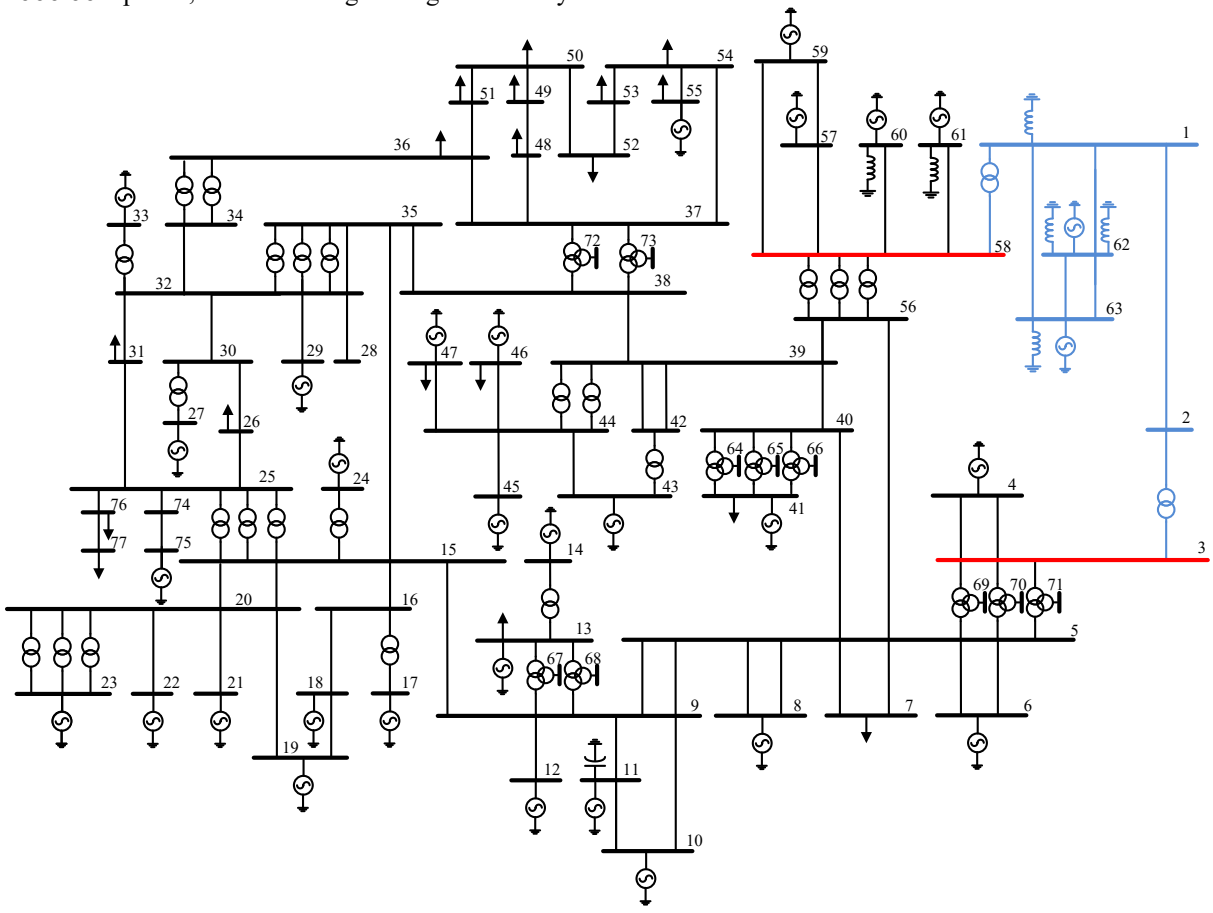

Fig. 12: 77-bus electrical network.

For the configuration shown in Fig. 13, the current measurement at the right-hand port allows the obtention of the self-admittance seen from this terminal ($y_{+1,1}(j\omega)$). Simultaneously, the short-circuit current measured at the left-hand port yields the transfer admittance between the left and right ports ($y_{+1,2}(j\omega)$). As there are only two ports in this example, the procedure should also be applied by inverting the ports to fully characterize the system, obtaining ($y_{+2,2}(j\omega)$) (note that $y_{+2,1}(j\omega)$ is equal to $y_{+1,2}(j\omega)$).

Fig. 14 and Fig. 15 show, respectively, the modulus and angle FRs of $y_{+1,1}$ considering the complete externa area model and the FDNE. The RMS error obtained in this comparison was 4.6394×10^{-4} %.

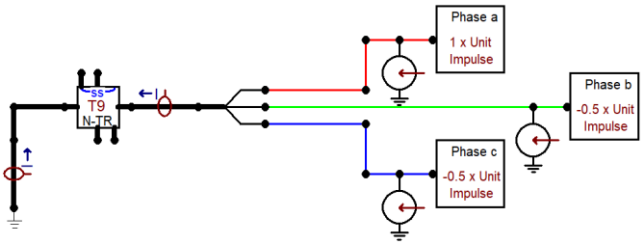

Fig. 13. Application of a balanced three-phase unit impulse voltage input in the two-ports FDNE implemented in ATP.

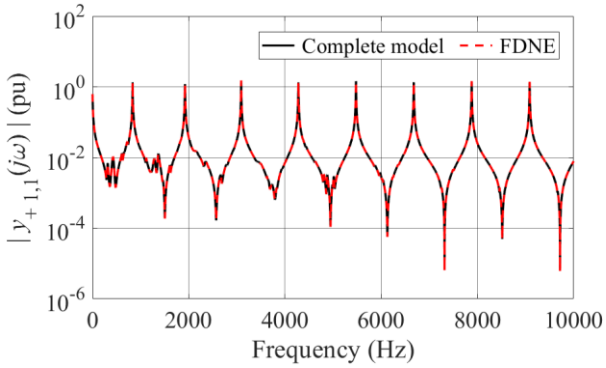

Fig. 14. $y_{+1,1}$ modulus FRs of the complete model and of the FDNE.

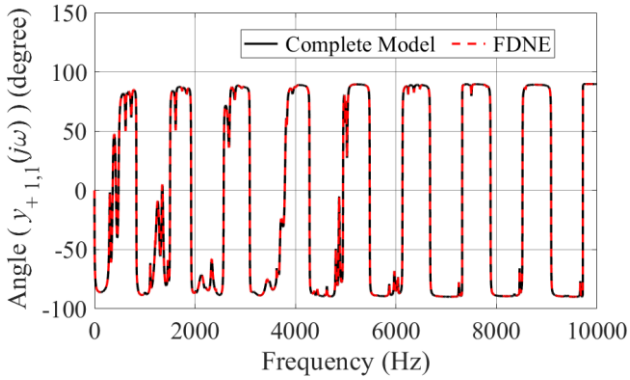

Fig. 15. $y_{+1,1}$ angle FRs of the complete model and of the FDNEs.

On the other hand, Fig. 16 and Fig. 17 show, respectively, the modulus and angle FRs of $y_{+1,2}$ considering the complete externa area model and the FDNE. The RMS error obtained in this comparison was 0.0074 %.

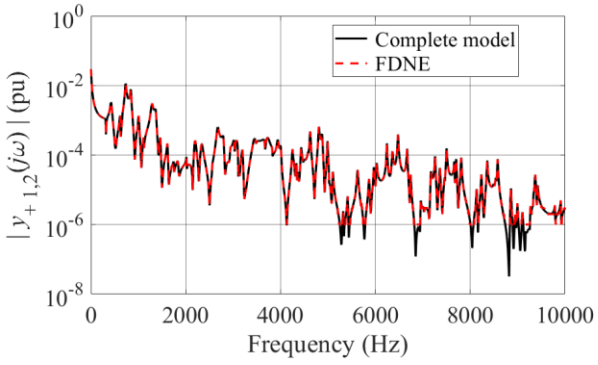

Fig. 16. $y_{+1,2}$ modulus FRs of the complete model and of the FDNE.

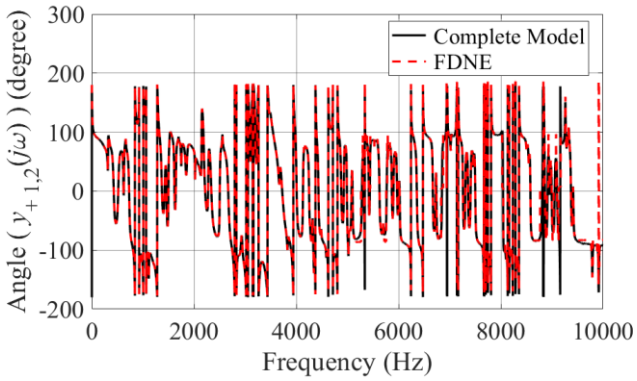

Fig. 17. $y_{+1,2}$ angle FRs of the complete model and of the FDNEs.

V. Conclusion

This work proposes a method for calculating the frequency responses of the UDMs implemented with the MODELS in the ATP. For this purpose, some important theoretical concepts were established, such as the UDM responses to three-phase unit impulse voltages.

Considerations on using a triangular function to obtain the UDM unit impulse responses are presented in detail.

Also, a highly efficient and simple-to-use NFTA was described in detail.

The proposed methodology was applied to obtain the FRs of two one-port BIPS FDNEs and one two-port 77-bus electrical network FDNE. Regarding the BIPS FDNEs, one is valid in the frequency range from 0 to 1.2 kHz, and the other is valid in the frequency range from 0 to 10 kHz. In the valid ranges, the FRs of the FDNEs show excellent agreement with that of the complete model. The two-port FDNE valid in the frequency range from 10 Hz to 10 kHz also shows excellent agreement with that of the full model, except for very low values of the transfer admittance ($y_{+1,2}$) due to accuracy limitations of the ATP software in the response calculation of a balanced three-phase unit impulse voltage input, reflected to the modulus and angle FRs.

Although in this work the emphasis was given to the positive sequence, the extension of the methodology to the zero sequence is straightforward.

References

[1] L. Dube and I. Bonfanti, "MODELS: A new simulation tool in the EMTP," *European Transactions on Electrical Power Engineering,* vol. 2, no. 1, pp. 45-50, 1992, http://dx.doi.org/10.1002/etep.4450020108.

[2] L. Prikler and H. K. Hoidalen, "ATPDraw Users Manual," 2009.

[3] R. G. F. Espinoza, F. B. Leao and J. R. S. Mantovani, "Simulation Environment of Distance Protection with ATP and Foreign Models," in *IEEE Electrical Power and Energy Conference*, Winnipeg, Canada, 2011, https://doi.org/10.1109/EPEC.2011.6070185.

[4] A. I. Chrysochos, A. I. Nousdilis, T. A. Papadopoulos and G. K. Papagiannis, "A Wide Band Black-Box Model of Power Transformers in ATP/MODELS," in *49th International Universities Power Engineering Conference (UPEC)*, Cluj-

Napoca, Romania, 2014, https://doi.org/10.1109/UPEC.2014.6934674.
[5] E. P. A. Ribeiro, F. V. Lopes, J. P. G. Ribeiro and E. J. S. Leite Jr., "ATP/MODELS Differentiator-Smoother Filter Model Validated Using Actual Time-Domain Relay," in *Workshop on Communication Networks and Power Systems (WCNPS)*, Brasília, Brazil, 2018, https://doi.org/10.1109/WCNPS.2018.8604374.
[6] R. Musca, G. Zizzo and A. Manunza, "Grid-Following and Grid-Forming MODELS in ATP-EMTP for Power Systems Simulation," in *AEIT International Annual Conference (AEIT)*, Rome, Italy, 2022, https://doi.org/10.23919/AEIT56783.2022.9951732.
[7] T. M. Campello, S. L. Varricchio and G. N. Taranto, "Representation of Multiport Rational Models in an Electromagnetic Transients Program: Networks with Lumped and Distributed Parameters," *Electric Power System Research,* vol. 178, 2020, https://doi.org/10.1016/j.epsr.2019.106029.
[8] T. M. Campello, S. L. Varricchio and G. N. Taranto, "Three-Phase Frequency-Dependent Network Equivalents in the ATP for Lumped Parameter Systems Using Descriptor Formulation, Rational Models, and Symmetrical Component Data," *Journal of Control, Automation and Electrical Systems,* vol. 32, pp. 1690-1703, 2021, https://doi.org/10.1007/s40313-021-00736-7.
[9] T. M. Campello, F. N. F. Dicler, S. L. Varricchio, H. M. de Barros, C. O. Costa, A. C. S. Lima and G. N. Taranto, "Reviewing the Large Electrical Network Equivalent Methods under Development for Electromagnetic Transient Studies in the Brazilian Interconnected Power System," *International Journal of Electrical Power and Energy Systems,* vol. 151, p. 109033, 2023, https://doi.org/10.1016/j.ijepes.2023.109033.
[10] B. Gustavsen and A. Semlyen, "Rational Approximation of Frequency Domain Responses by Vector Fitting," *IEEE Transactions on Power Delivery,* vol. 14, no. 3, pp. 1052 - 1061, Julho 1999, https://doi.org/10.1109/61.772353.
[11] B. Gustavsen and H. M. J. D. Silva, "Inclusion of Rational Models in an Electromagnetic Transient Program: Y-Parameters, Z-Parameters, S-Parameters, Transfer Functions," *IEEE Transactions on Power Delivery,* vol. 28, no. 2, pp. 1164 - 1174, 2013, https://doi.org/10.1109/TPWRD.2013.2247067.
[12] J. M. Rodriguez, E. Medina, J. Mahseredjian, A. Ramirez, K. Sheshyekani and I. Kocar, "Frequency-Domain Fitting Techniques: A Review," *IEEE Transactions on Power Delivery,* vol. 35, no. 3, pp. 1102-11010, 2020, https://doi.org/10.1109/TPWRD.2019.2932395.
[13] W. Bolton, Instrumentation and Control Systems, Elsevier Ltd, 2006, https://doi.org/10.1016/C2020-0-00286-0.
[14] M. Frigo and S. Johnson, "FFTW: An Adaptive Software Architecture for the FFT," in *IEEE International Conference on Acoustics, Speech and Signal Processing, ICASSP*, Seattle, USA, 1998, https://doi.org/10.1109/ICASSP.1998.681704.
[15] S. G. Johnson and M. Frigo, "A Modified Split-Radix FFT with Fewer Arithmetic Operations," *IEEE Transactions on Signal Processing,* vol. 55, no. 1, pp. 111-119, 2007, https://doi.org/10.1109/TSP.2006.882087.
[16] MathWorks, "Matlab," [Online]. Available: https://www.mathworks.com/products/matlab.html.
[17] Y. Du, S. C. Liew and Y. Shao, "Efficient FFT Computation in IFDMA Transceivers," *IEEE Transactions on Wireless Communications,* vol. 22, no. 10, pp. 6594-6607, 2023, https://doi.org/10.1109/TWC.2023.3244553.
[18] N. Malladhi, K. N. Reddy and R. R. Vallabhuni, "Novel architecture of FFT implementation for 5G module using machine learning algorithms," *International Journal of System Assurance Engineering and Management,* vol. 14, p. 2387–2394, 2023, https://doi.org/10.1007/s13198-023-02087-9.
[19] H. Ogata, "Numerical calculation of Fourier transforms based on hyperfunction theory," *Journal of Computational and Applied Mathematics,* vol. 378, p. 112921, 2020, https://doi.org/10.1016/j.cam.2020.112921.
[20] S. L. Varricchio, S. Gomes Jr. and R. D. Rangel, "Three Winding Transformer s-Domain Model for Modal Analysis," *International Jounal of Electrical Power and Energy Systems,* pp. 420-429, 2011, https://doi.org/10.1016/j.ijepes.2010.10.003.
[21] C. M. Close, The Analysis of Linear Circuits, San Diego, USA: Hard-Court Brace Jovanovich Inc., 1966.
[22] M. R. Spiegel and J. Liu, Mathematical handbook of formulas and tables, 2nd ed., New York, USA: Mc-Graw Hill, 1998, http://dx.doi.org/10.1036/0071548556.
[23] ONS, "SINtegre: Portal de Relacionamento," [Online]. Available: https://sintegre.ons.org.br. [Accessed 05 05 2024].

Sergio Luis Varricchio (SM'06) received the B.Sc. degree from the Catholic University of Petrópolis (UCP), Petrópolis, Brazil, in 1987, the M.Sc. degree from the Federal University of Rio de Janeiro (UFRJ), Rio de Janeiro, Brazil, in 1994, and the Ph.D. degree from the University of Brasília, DF, Brazil, in 2015, all in electrical engineering. From 1989 to 2024, when he retired, he worked at CEPEL, Rio de Janeiro, Brazil, as a project manager and researcher in the areas of modal analysis, model order reduction, power quality and electromagnetic transients. Currently, he works as an independent consultant.

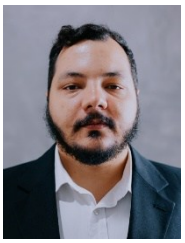

Thomas M. Campello (Member, IEEE), holds a bachelor's degree (2016) and a master's degree (2018) in Electrical Engineering with a focus on Power Systems from the Federal Fluminense University (UFF) and the Federal University of Rio de Janeiro (COPPE/UFRJ), respectively. He is currently pursuing a PhD at COPPE/UFRJ in the same field. He is also a professor at the Federal Center for Technological Education Celso Suckow da Fonseca (CEFET/RJ). His interests include Scientific Computing, Power Quality, Modal Analysis, Mathematical Modeling of Electrical Equipment, Model Order Reduction, and Electromagnetic Transients.